












All-Season Liquid Soil Moisture Retrieval From SMAP

Chi Wang , Na Yang , Tianjie Zhao , *Senior Member, IEEE*, Huazhu Xue , Zhiqing Peng , Jingyao Zheng, Jinmei Pan , Panpan Yao , Xiaowen Gao, Hongbo Yan , Peilin Song , Yuei-An Liou , *Senior Member, IEEE*, and Jiancheng Shi , *Fellow, IEEE*

Abstract—In cold regions, the coexistence and interconversion of liquid water and ice in frozen soils have important implications for energy partitioning and surface runoff at the Earth's surface. Passive microwave remote sensing is crucial for the global monitoring of soil moisture (SM). However, current research on SM focuses mainly on unfrozen soil conditions. Limited studies have been conducted on variations in soil liquid water content throughout the freezing season. This article investigated the potential use of brightness temperature observations from the Soil Moisture Active Passive (SMAP) satellite for retrieving all-season liquid SM. The single-channel algorithm and the Zhang-Zhao dielectric model, which was specifically developed for freezing and thawing soils, achieved successful retrieval of liquid SM in both frozen and thawed soils, even when snow cover was present. The results indicate improved spatial coverage (during winter) and consistent spatial patterns in SM compared with the SMAP products. Validation at 17 SM networks suggests that the retrieved all-season liquid SM effectively captures the dynamic characteristics of each region with an average bias of $0.011 \text{ m}^3/\text{m}^3$, an average unbiased root mean square error of $0.056 \text{ m}^3/\text{m}^3$, and an average correlation coefficient of 0.76. The additional retrieval of unfrozen water content during the freezing season would enhance the monitoring and understanding of the hydrological cycle and energy balance in cold regions.

Index Terms—Liquid water content, microwave remote sensing, soil moisture active passive (SMAP), soil moisture (SM).

I. INTRODUCTION

SOIL moisture (SM) is the total water content in the soil, which exists in liquid, solid, and gaseous forms. Soil freezes when its temperature falls below 0°C . However, due to surface tension and solutes in the SM, water in the frozen soil always remains in a certain amount of liquid state [1]. This liquid form of water is called unfrozen water. In seasonal frozen ground, unfrozen water and ice coexist, and their interconversion, known as freeze-thaw changes, affects hydrological, ecological, infrastructural, and climatic feedbacks, as well as having far-reaching impacts on the global carbon cycle and climate dynamics. The large energy-water transitions associated with surface freezing and thawing alter heat distribution in the soil, leading to complex interactions between the soil and the surrounding air. When water freezes, it releases latent heat to the surrounding area, causing a localized temperature increase [2]. Conversely, when ice thaws, it absorbs heat from its surroundings, resulting a decrease in temperature. These energy-water transformations play a crucial role in shaping various environmental processes. In addition, the hydraulic conductivity of frozen soil can be significantly reduced, resulting in different patterns of flow production and sink, which in turn change the characteristics of the wider regional water cycle [3], [4]. Monitoring changes in unfrozen water and freeze-thaw in surface soils is crucial to characterize hydrological changes in frozen soils under climate change scenarios.

Ground-based SM observations provide a precise understanding of unfrozen water and freeze-thaw alterations in soil [5]. However, current region-specific ground-based observation networks face significant spatial heterogeneity, making them inadequate for global or regional monitoring of unfrozen water and freeze-thaw changes in soil distribution characteristics [6].

Microwave remote sensing technology obtains soil surface information by measuring reflected, scattered, and radiated microwave signals. Microwave signals can be used to infer the liquid water content and freeze-thaw state of the soil [7], [8]. Following the successful deployment of the Soil Moisture and Ocean Salinity (SMOS) [9], [10] and Soil Moisture Active Passive (SMAP) [11], [12] satellites, SM products have been progressively utilized in a variety of hydrological and ecological studies. Simultaneously, this has also contributed to the research boom in monitoring surface soil freeze-thaw

Manuscript received 4 December 2023; revised 16 February 2024; accepted 13 March 2024. Date of publication 28 March 2024; date of current version 19 April 2024. This work was supported in part by the National Key Research and Development Program of China under Grant 2021YFB3900104, and in part by the National Natural Science Foundation of China under Grant 42201393. (Corresponding author: Tianjie Zhao.)

Chi Wang, Na Yang, and Huazhu Xue are with the School of Surveying and Land Information Engineering, Henan Polytechnic University, Jiaozuo 454000, China (e-mail: 212104020011@hpu.edu.cn; yangna@hpu.edu.cn; xhz@hpu.edu.cn).

Tianjie Zhao, Zhiqing Peng, Jingyao Zheng, Panpan Yao, and Xiaowen Gao are with the State Key Laboratory of Remote Sensing Science, Aerospace Information Research Institute, Chinese Academy of Sciences, and University of Chinese Academy of Sciences, Beijing 100101, China (e-mail: zhaotj@aircas.ac.cn).

Jinmei Pan and Jiancheng Shi are with the National Space Science Center, Chinese Academy of Sciences, Beijing 100190, China (e-mail: shijiancheng@nssc.ac.cn).

Hongbo Yan is with the Guilin University of Technology, Guilin 541004, China.

Peilin Song is with Xi'an Jiaotong University, Xi'an 710049, China.

Yuei-An Liou is with Hydrology Remote Sensing Laboratory, Center for Space and Remote Sensing Research, National Central University, Taoyuan 320317, Taiwan (e-mail: yueian@csrsl.ncu.edu.tw).

Digital Object Identifier 10.1109/JSTARS.2024.3382315

alterations through L-band passive microwave remote sensing [11]. The greater penetration of the L-band will greatly simplify the interpretation of areas with important vegetation [1]. However, current SM products, such as SMOS and SMAP, do not provide sufficient information on changes in the water content of frozen soil. In addition, freeze/thaw products are effective in identifying whether surface soil in a given area has experienced a freezing or thawing event, but fail to provide insight into temporal changes in the distribution of liquid water in frozen soils [13].

The availability of microwave remote sensing tools for monitoring unfrozen water in frozen soils is limited, mainly because the current soil dielectric constant models are not applicable to frozen soils. These models developed by Dobson et al. [14] and Mironov et al. [15] are only applicable to SM retrieval in nonfrozen soils. In recent years, there has been a gradual rise in dielectric constants modeling during freeze-thaw transitions to aid the remote sensing of seasonal frozen ground characteristics. Schwank et al. [16] conducted a preliminary validation of the four-phase hybrid dielectric constant model originally proposed by Birchak et al. [17] to assess its applicability. In addition, Mironov worked on the dielectric modeling of seasonal frozen ground. The authors in [18] and [19] investigated the phase transition process of different types of water in clay and evaluated the dielectric properties of wet bentonite samples at positive and negative temperatures. The authors in [20] and [21] developed a temperature-dependent multiple relaxation spectral medium model based on their measurements of organic matter-rich soil samples. In 2017, Mironov et al. [22] developed a model based on a single frequency using dielectric measurements from three representative soils collected from the Yamal Peninsula. More recently, Mironov et al. [23] developed a dielectric model applicable to both unfrozen and frozen mineral soils found in the Arctic tundra. However, Mironov's model exhibits a discontinuity during the freeze-thaw transition, where it assumes that all the water in the soil is either freezing or thawing [24]. Zhang et al. [25] proposed an innovative approach that combines the Dobson model with the correlation between unfrozen water content, specific surface area (SSA), and soil texture. This improves the simulation accuracy of the model.

Zhao et al. [26] introduced a novel parametric approach to establish the correlation between unfrozen water, soil temperature, and initial SM. Wu et al. [27] validated the new scheme using dielectric measurements from six types of soil samples. This model is now referred to as the Zhang-Zhao model. Recent developments in the dielectric modeling of frozen soils have facilitated the retrieval of liquid water content, which also allows the retrieval of SM during periods of soil freezing.

This study is based on a zero-order approximation microwave radiation transmission model (τ - ω) [28]. The single-channel algorithm (SCA) is used in conjunction with the Zhang-Zhao dielectric model to retrieve the unfrozen water content from SMAP observations. The accuracy is evaluated over 17 global SM observing networks. In Section II, this article presents the data of brightness temperature and the ground measurements. The methodology of the radiative transfer model and SM retrieval algorithm implemented in this study are described in

Section III. Section IV presents the results and the discussion of the shortcomings, as well as the directions for the future expansion of this study. Finally, Section V presents conclusions.

II. DATA

A. Brightness Temperature

This study uses brightness temperature (TB) data provided by the SMAP products (L3_SM_P) with a spatial resolution of 36 km. The data can be downloaded from the National Snow and Ice Data Centre (NSIDC)¹. Only ascending orbit data were used. For this study, TB observations from SMAP satellites were selected for the periods from January 2017 to December 2017 and from January 2020 to December 2020.

B. In-Situ SM Data

Ground measurements of SM serve as a benchmark. Incorporating this validated data into the evaluation process allows the determination with a high degree of confidence whether our methods accurately reflect real-world conditions. It also allows to identify any potential biases or limitations in the methods, and to make necessary adjustments and improvements. These data come from the International Soil Moisture Network [29], the United States Department of Agriculture watersheds, and the National Tibetan Plateau Data Center [30]. SM networks are distributed across regions with different climatic conditions, temperature ranges, precipitation patterns, and seasonal fluctuations. The networks also cover different types of land cover, with multiple soil types taken into account in their design. These networks play a critical role in validating and refining data obtained through remote sensing technologies [31], [32]. Fig. 1 shows the global distribution of these sites. The base map data are from Natural Earth.² Table I presents the details of the soil moisture networks selected for this study, including their center's latitude and longitude, climatic conditions, and location by country or region.

C. Other Data

Sand and clay fractions for soil dielectric modeling were obtained from the Global SoilGrids database (SoilGrids250m) [33]. Several ancillary datasets from the SMAP product (L3_SM_P) were also used, including surface soil temperature (T_{eff}), single scattering albedo of vegetation (ω_p), and vegetation water content (VWC). Land cover types are based on the International Geosphere-Biosphere Programme (IGBP) [34].

Snow density (ρ_{snow}), temperature of snow layer (T_{snow}), and snow depth (S_{depth}) data were obtained from ERA5 - Land Hourly Snow Data [35]. Snow density data were excluded by setting thresholds, dropping snow depths less than 3 cm, and snow layer temperatures greater than 0°C (indicating wet snow).

¹[Online]. Available: <https://nsidc.org/data/smap/smap-data.html>.

²[Online]. Available: <https://www.naturalearthdata.com/downloads/50m-raster-data/50m-natural-earth-1/>.

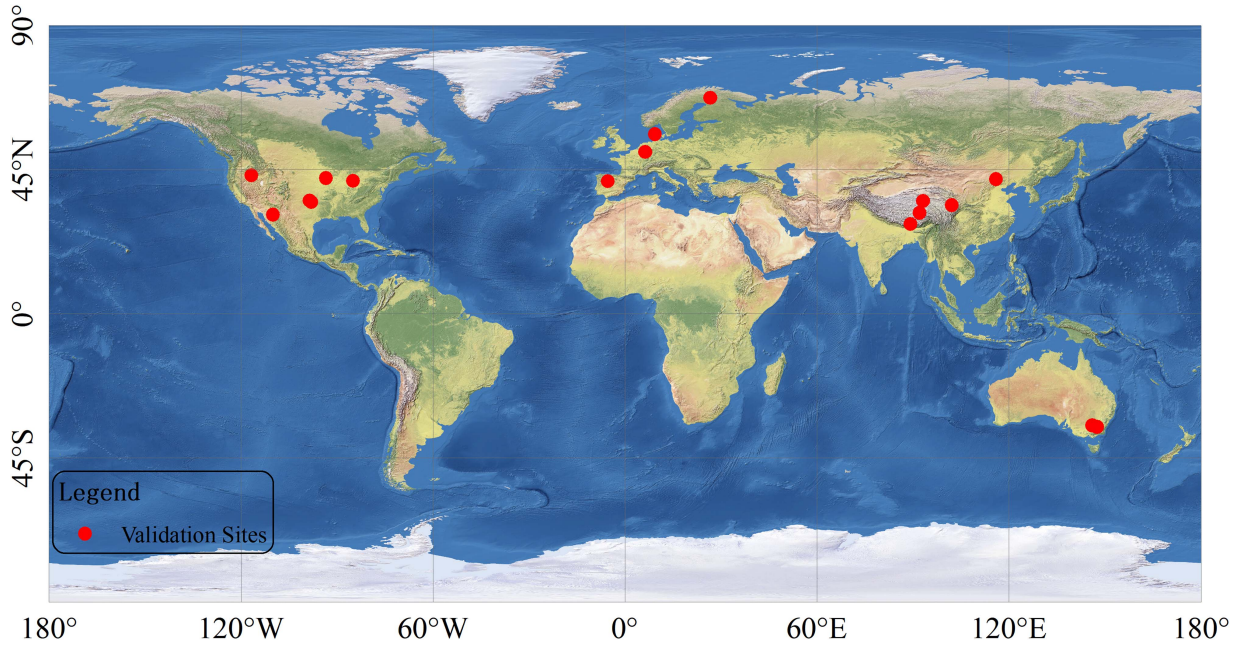


Fig. 1. Location of in-situ SM validation sites.

TABLE I
DETAILS REGARDING THE SELECTED IN-SITU SM NETWORKS

Site name	Location	Climate regime	Center coordinates	Sensor numbers	Data period used
Maqu	China	Cold	33.88°N,102.13°E	10	2017/01/01–2017/12/31
Naqu	China	Polar	31.49°N,92.07°E	34	2017/01/01–2017/12/31
Pali	China	Arid	27.95°N,89.19°E	8	2017/01/01–2017/12/31
SMN-SDR	China	Cold	42.00°N,116.00°E	33	2020/01/01–2017/12/31
SMN-WDL	China	Cold	35.18°N,93.14°E	10	2020/01/01–2017/12/31
FMI	Finland	Cold	67.368°N,26.633°E	14	2017/01/01–2017/12/31
HOBE	Denmark	Temperate	56.074°N,9.334°E	25	2017/01/01–2017/12/31
Oznet-Kyeamba	Australia	Temperate	35.26°S,147.456°E	6	2017/01/01–2017/12/31
Oznet-Yanco	Australia	Semiarid	34.87°S,146.13°E	11	2017/01/01–2017/12/31
REMEDHUS	Spain	Temperate	41.31°N,5.38°W	20	2017/01/01–2017/12/31
TERENO	Germany	Temperate	50.5°N,6.33°E	4	2017/01/01–2017/12/31
Fort-Cobb	USA	Temperate	35.34°N,98.57°W	14	2017/01/01–2017/12/31
Little-Washita	USA	Temperate	34.88°N,98.08°W	19	2017/01/01–2017/12/31
South-Fork	USA	Cold	42.44°N,93.44°W	20	2017/01/01–2017/12/31
St.-Josephs	USA	Cold	41.449°N,85.011°W	10	2017/01/01–2017/12/31
Reynolds-Creek	USA	Arid	43.188°N,116.748°W	18	2017/01/01–2017/12/31
Walnut-Gulch	USA	Arid	31.72°N,110.05°W	27	2017/01/01–2017/12/31

Sensor numbers refer to the maximum station of a network in the validation period.

III. METHODS

A. Microwave Emission Models

Microwave emissions at the Earth's surface are influenced by factors, such as the atmosphere, surface cover (including vegetation and snow), and surface roughness. In particular, the effects of vegetation and snow on microwaves are highly complex, as they can exhibit strong absorption and scattering properties within them. For accurate SM retrieval, algorithms typically focus on separating the interactions between the soil and the surface cover of vegetation or snow. At L-band, the atmosphere and dry snow are relatively transparent to microwaves, and their effects can be ignored. Therefore, the observed total TB can be

simplified as follows [27], [36]:

$$TB_p = T_{soil}\gamma_p(1 - r_{soil,p}) + (1 - \omega_p)(1 - \gamma_p)(1 + \gamma_p r_{soil,p})T_c \quad (1)$$

where p is the polarization. ω_p is the single scattering albedo. γ_p is the vegetation transmissivity ($\gamma_p = \exp(-\tau_p / \cos \theta)$, θ is the angle of incidence relative to nadir, for SMAP, where $\theta = 40^\circ$). T_c and T_{soil} are the effective canopy and soil temperatures, respectively. Assuming thermal equilibrium between the vegetation and soil, their values can be assumed to be approximately equal to T_{eff} . $r_{soil,p}$ is the reflectivity at the rough soil surface as a function of the incidence angle just above the soil boundary

and the roughness of the reflecting interface [37], [38], [39].

$$\Gamma_{\text{soil,p}} = R_{\text{soil,p}} \cdot H_p(\theta) \quad (2)$$

where $R_{\text{soil,p}}$ is the soil specular reflectance from a flat surface.

$$R_{\text{soil,H}}(\theta) = \left| \frac{\cos(\theta) - \sqrt{\varepsilon_r - \sin^2(\theta)}}{\cos(\theta) + \sqrt{\varepsilon_r - \sin^2(\theta)}} \right|^2$$

$$R_{\text{soil,V}}(\theta) = \left| \frac{\varepsilon_r \cos(\theta) - \sqrt{\varepsilon_r - \sin^2(\theta)}}{\varepsilon_r \cos(\theta) + \sqrt{\varepsilon_r - \sin^2(\theta)}} \right|^2 \quad (3)$$

where θ is the incidence angle relative to nadir. ε_r is the relative permittivity. In cases where there is no snow cover on the soil surface, $\theta = \theta_{\text{soil}}^{\text{air}}$ (for SMAP, where $\theta_{\text{soil}}^{\text{air}} = 40^\circ$), $\varepsilon_r = \frac{\varepsilon_{\text{soil}}}{\varepsilon_{\text{air}}}$ ($\varepsilon_{\text{air}} = 1$). If the soil surface is covered with snow, the snow layer is transparent for L-band because dry snow has a minimal absorption that can be neglected. In addition, the small scattering at the interface of the snow layer can also be neglected. Therefore, we consider the snow layer as a single layer, and the soil and air layers as semi-infinite spaces. The layering effect of the snow is not explicitly considered. We mainly consider the refractive effects of the snow on the incidence angle and the relative permittivity. For this time, the propagation angle ($\theta = \theta_{\text{soil}}^{\text{snow}}$) inside the snow is a function of the incidence angle ($\theta_{\text{soil}}^{\text{air}} = 40^\circ$) [40].

$$\theta_{\text{soil}}^{\text{snow}} = \arcsin \frac{\sin(\theta_{\text{soil}}^{\text{air}})}{\sqrt{\varepsilon_{\text{snow}}(\rho_{\text{snow}})}} \quad (4)$$

$$\varepsilon_r = \frac{\varepsilon_{\text{soil}}}{\varepsilon_{\text{snow}}} \quad (5)$$

$\varepsilon_{\text{snow}}$ is the complex dielectric constant of the snow cover, which is a function of the snow density (ρ_{snow}) [40].

$\varepsilon_{\text{snow}} =$

$$\begin{cases} 1 + 1.5995 \cdot \rho_{\text{snow}} + 1.861 \cdot (\rho_{\text{snow}})^3 \\ 0 \text{ g} \cdot \text{cm}^{-3} \leq \rho_{\text{snow}} \leq 0.4 \text{ g} \cdot \text{cm}^{-3} \\ (0.99913 \cdot (1 - \rho_{\text{snow}}/0.917) + \rho_{\text{snow}}/0.917 \cdot 1.4759)^3 \\ \rho_{\text{snow}} > 0.4 \text{ g} \cdot \text{cm}^{-3} \end{cases} \quad (6)$$

To better understand this process, we have created a forward soil-snow-canopy emission model in the L-band, as shown in Fig. 2.

In this study, a simple parameter called H_p is used to represent the effect of roughness at different angles of incidence [41]. The formula is as follows:

$$H_p = A_p \cdot \exp(B_p \cdot m^2 + C_p \cdot m) \quad (7)$$

$$m = s^2/l \quad (8)$$

$$A_p, B_p, C_p = a \cdot \theta^2 + b \cdot \theta + c \quad (9)$$

where s is the root mean square height, l is the correlation length, and m is defined as the slope. θ is the incidence angle relative to the nadir of the ground surface. Snow free conditions $\theta = \theta_{\text{soil}}^{\text{air}}$, snow covered conditions $\theta = \theta_{\text{soil}}^{\text{snow}}$.

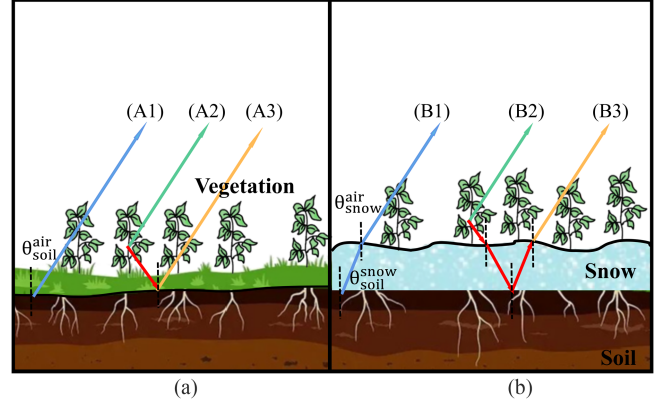


Fig. 2. Schematic diagram of the transmission process of microwave emissions on the surface of the Earth. (a) Snowless conditions. (b) Snow-covered conditions.

B. Zhang-Zhao Model

The dielectric constant of frozen and thawed soils using the Zhang-Zhao model is calculated as follows [25], [27]:

$$\varepsilon_{\text{total}}^{\prime\alpha} = \begin{cases} 1 + \frac{\rho_b}{\rho_s} (\varepsilon_s^{\prime\alpha} - 1) + m_{vl}^{\beta'} \varepsilon_{lw}^{\prime\alpha} - m_{vl}; & T > 0^\circ\text{C} \\ 1 + \frac{\rho_b}{\rho_s} (\varepsilon_s^{\prime\alpha} - 1) + m_{vl}^{\beta'} \varepsilon_{lw}^{\prime\alpha} - m_{vl} \\ + m_{vi} \varepsilon_i^{\prime\alpha} - m_{vi}; & T \leq 0^\circ\text{C} \end{cases} \quad (10)$$

$$\varepsilon_{\text{total}}^{\prime\prime\alpha} = m_{vl}^{\beta''} \varepsilon_{lw}^{\prime\prime\alpha} \quad (11)$$

where ε' and ε'' are the real and imaginary components of the complex permittivity. The subscripts s , lw , and i refer to solids in the soil, liquid water, and ice, in that order. ρ_b is the bulk density. ρ_s is the specific density. m_v is the volumetric water content of the soil. The subscript l refers to liquid SM. The α is the shape factor constant. We made further modifications to the parameters (soil temperatures $\geq 0^\circ\text{C}$, $\alpha = 0.85$, soil temperatures $< 0^\circ$, $\alpha = 0.56$) using global soil texture data based on Wu et al. [27]. m_{vu} is the unfrozen water expressed as follows [26]:

$$m_{vu} = m_{v,\min} + (m_{v,\max} - m_{v,\min}) \cdot e^{(-K \cdot |T_{\text{eff}}|)} \quad (12)$$

$m_{v,\max}$ is the total water content in the soil. $m_{v,\min}$ is the fraction of water that is permanently unfrozen when the soil freezes, also known as the maximum bound water content [21].

$$m_{v,\min} = (0.0016 + 0.0017 \cdot CL) \cdot \left(1 + 1.2472 \cdot e^{\frac{T_{\text{soil}}}{7.1932}} \right). \quad (13)$$

The Zhang-Zhao model introduces an SSA representing the soil surface tension to determine the parameter K . According to the physical meaning of the unfrozen water content equation, the value of K depends on the applied freezing rate of soil liquid water. Soils with a high SSA have an increased amount of bound water and a reduced amount of free water. The particles in the soil have a strong bond with the bound water, resulting in a slower freezing rate compared to the free water. Therefore, it can be observed that soils with a high SSA tend to freeze at a comparatively lower temperature and have a slower freezing rate. Based on the above-mentioned physical definition, K and

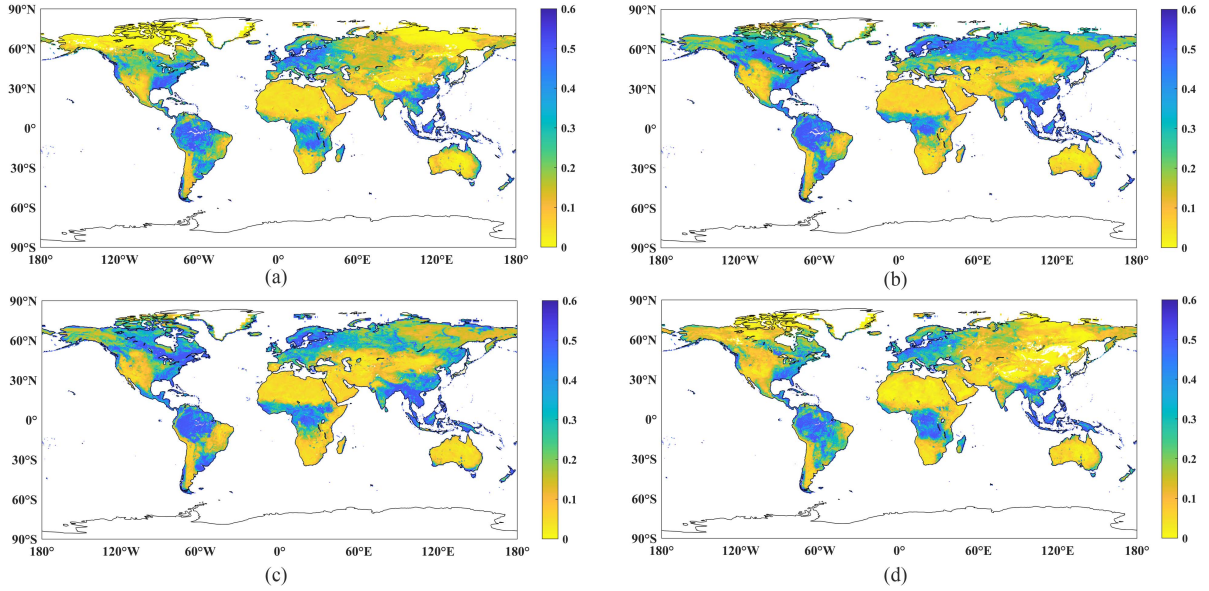


Fig. 3. Global liquid SM maps of monthly average. (a) March. (b) June. (c) September. (d) December.

SSA [42] are determined in the form of a power function as follows:

$$K = a \cdot SSA^b \quad (14)$$

$$SSA = 0.042 + 4.23CL + 1.12SL - 1.16SD \quad (15)$$

where CL, SL, and SD represent the percentages of clay, silt, and sand, respectively.

C. Single-Channel Algorithm

In the SCA, the TB is first converted to emissivity using the surface temperature [43].

$$e_p^{total} = \frac{TB_p}{T_{eff}} \quad (16)$$

Emissivity is commonly thought to be affected by both vegetation and surface roughness. We first consider eliminating the influence of vegetation through the single scattering albedo (ω_p) of vegetation and the vegetation transmittance (γ_p).

The γ_p is a function of the τ . The τ depends on the VWC [44].

$$\gamma_p = \exp(-\tau_p / \cos \theta) \quad (17)$$

$$\tau_p = b_p \cdot VWC. \quad (18)$$

The b_p parameter is obtained from the parameter table of the IGBP class lookup algorithm in ATBD [43]. θ is the incidence angle relative to nadir (for SMAP, where $\theta = 40^\circ$).

By rearranging Equation (1), the effects of vegetation are eliminated using the single scattering albedo and optical thickness of vegetation. The emissivity $e_{soil,p}$ of a rough surface can be calculated using the following formula [43]:

$$e_{soil,p} = \frac{e_p^{total} - 1 + \gamma_p^2 + \omega_p - \omega_p \cdot \gamma_p^2}{\gamma_p^2 + \omega_p \cdot \gamma_p - \omega_p \cdot \gamma_p} \quad (19)$$

The reflectivity of the soil surface ($r_{soil,p}$) can be obtained by subtracting the reflectivity from 1.

$$r_{soil,p} = 1 - e_{soil,p} \quad (20)$$

At this point, the effective reflectance of the ground is influenced by both the surface roughness and the angle. This influence is eliminated by the roughness parameter ($H_p(\theta)$) and the specular reflectance of the soil ($R_{soil,p}(\theta, \varepsilon_r)$) is obtained.

$$R_{soil,p} = \frac{r_{soil,p}}{H_p(\theta)}. \quad (21)$$

The roughness parameter $H_p(\theta)$ should be considered in two scenarios. Snow free conditions $\theta = \theta_{soil}^{air}$, snow-covered conditions $\theta = \theta_{soil}^{snow}$. Using the Fresnel equations, the relative dielectric constant of the soil can be obtained.

$$\varepsilon_{r,H} = \sin^2(\theta) + \left(\cos(\theta) \cdot \frac{-1 - \sqrt{R_{soil,H}}}{\sqrt{R_{soil,H} + 1}} \right)^2 \quad (22)$$

$$\varepsilon_{r,V} = \frac{a2 + \sqrt{(a2)^2 - 4\sin^2(\theta) \cdot \cos^2(\theta) \cdot (a1) \cdot (a2)}}{2\cos^2(\theta) \cdot (a1)} \quad (23)$$

where $a1 = (1 - \sqrt{R_{soil,V}})^2$, $a2 = (1 + \sqrt{R_{soil,V}})^2$. Snowless conditions $\theta = \theta_{soil}^{air}$, $\varepsilon_{soil} = \varepsilon_{r,P} \cdot \varepsilon_{air}$, Snow-covered conditions $\theta = \theta_{soil}^{snow}$, $\varepsilon_{soil} = \varepsilon_{r,P} \cdot \varepsilon_{snow}$.

With the complex dielectric constant of the soil, the liquid SM content can be obtained through a soil dielectric model. All results in this article are based on the SCA-V algorithm.

IV. RESULTS AND DISCUSSION

A. Global Spatial Distribution of Retrieval Results

To assess the spatial and temporal reliability of the liquid SM retrieval results, global-scale SM maps were generated for

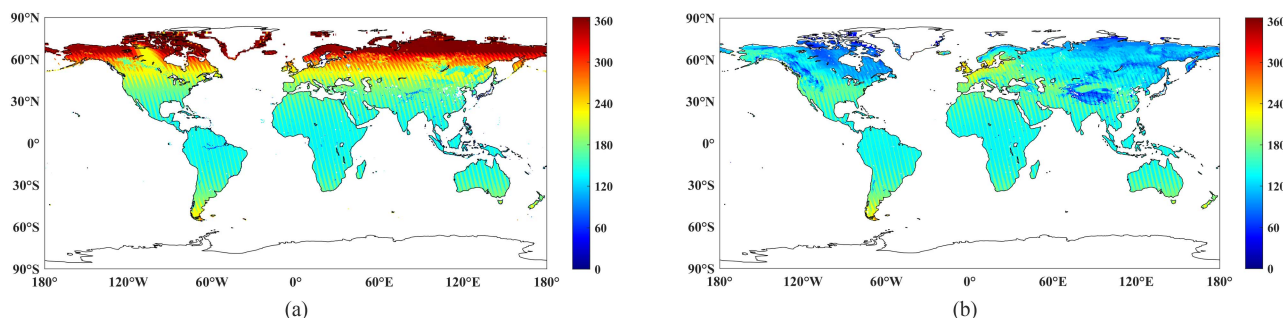


Fig. 4. Number of SM retrievals over each grid in one year (2017). (a) New retrieval. (b) SMAP.

some months of 2017, including March (spring), June (summer), September (autumn), and December (winter). These maps illustrate the monthly mean values of liquid SM (Fig. 3).

In particular, liquid SM was retrieved in regions with seasonally frozen ground and permafrost, such as the mid- to high-latitude regions of Eurasia and North America, as well as the Tibetan Plateau region of China [12].

Seasonal variations in SM are evident in the northern parts of North America and Siberia. In winter, SM is low due to low temperatures and snowfall, resulting in soil freezing in most areas. In spring and summer, SM increases due to rising temperatures, soil thawing, and increased precipitation. SM then decreases slightly in autumn compared to summer. In the Mediterranean, summers are characterized by scorching and dry conditions with minimal rainfall.

There is a decrease in SM during the summer, which then recovers in the winter due to increased precipitation. Arid and desert regions, such as the Sahara Desert in Africa and the Australian Outback, experience persistently dry conditions and have low SM. Due to minimal rainfall and significant evapotranspiration, SM remains consistently low and fairly stable. The Amazon Rain Forest region of South America experiences high levels of rainfall throughout the year, resulting in consistently high levels of SM. During the summer and autumn months in Central Africa, regions north of the equator experience higher levels of precipitation due to the influence of the Indian Ocean monsoon. As a result, these regions have higher SM. In contrast, areas t south of the equator have lower SM. This phenomenon is gradually reversed during the spring and winter, with precipitation patterns shifting southwards. Consequently, SM content increases in locations south of the equator, while areas north of the equator become increasingly arid. The retrieval algorithm used in this study is not only applicable to seasonal frozen ground and permafrost zones, but also to other climatic zones. It is capable of capturing their general trends and the dynamics of SM.

Fig. 4. shows the global distribution of the number of SM retrievals in each grid over the course of a year, using 2017 as an example. Typically, our annual dataset contains more than 200 retrievals. SMAP retrieves SM on average 150 times per year. However, in the northernmost regions of Eurasia and North America, as well as on the Tibetan Plateau in China, the occurrence of SM is less frequent, largely due to the flagging of frozen soils.

B. Validation Using In-Situ Measurements

Time series and scatter plots of the retrieved SM are shown in Figs. 5–7. Statistical indicators for the 17 sites are shown in Table II. The measured value at the site is represented by the black line. The green dots represent the retrieved values after accounting for the effect of snow, while the black circles represent the retrieved values without accounting for the effect of snow. Our aim is to assess the reliability of the retrieved SM data in comparison to ground-based observations, as well as their ability to accurately capture the variations in liquid SM content over different seasons.

There are five SM validation networks in China (Maqu, Naqu, Pali, SMN-SDR, and SMN-WDL). Among them, Maqu, Naqu, Pali, and SMN-WDL are located in high altitude areas (third pole). The results in low temperatures which pose a challenge to the liquid SM retrieval algorithm. The average duration of successful retrieval in these regions reached 180 days.

The Maqu network was established in the semiarid region on the eastern edge of the Qinghai Plateau in Tibet [45]. This region is featured by variable rainfall and warmth in summer, and drought and cold in winter. The annual precipitation is close to 600 mm. The occurrence of freeze-thaw cycles is common when wetness is high in winter and spring. With a higher SM, the contrast between in situ and retrieved became more pronounced during summer and autumn. Associated with a higher SM, the increase in errors may be caused by rain and land management, which can affect soil emissivity early in the growing season.

The Naqu network was located in a cold, semiarid climate zone with aridity [29]. Between October and March, the site experienced a freeze-thaw cycle, resulting in a gradual reduction of liquid moisture in the soil as it froze. From December to March, the soil froze completely and remained in a stable state. As the temperature rises and the soil gradually thaws by April, the moisture content of the soil begins to increase as a result of the melting of the ice. The results of our retrieval slightly underestimate the amount of water in the soil, but they accurately represent the variations in freezing and thawing.

The Pali network is located in the flat terrain surrounding Pali town in Yadong county, while Pali town is located in the Yadong valley of the Himalayas [46]. This area has a hilly environment with mostly bare ground and sparse grasses covering the land. The average altitude in this region is 4486 m and the annual

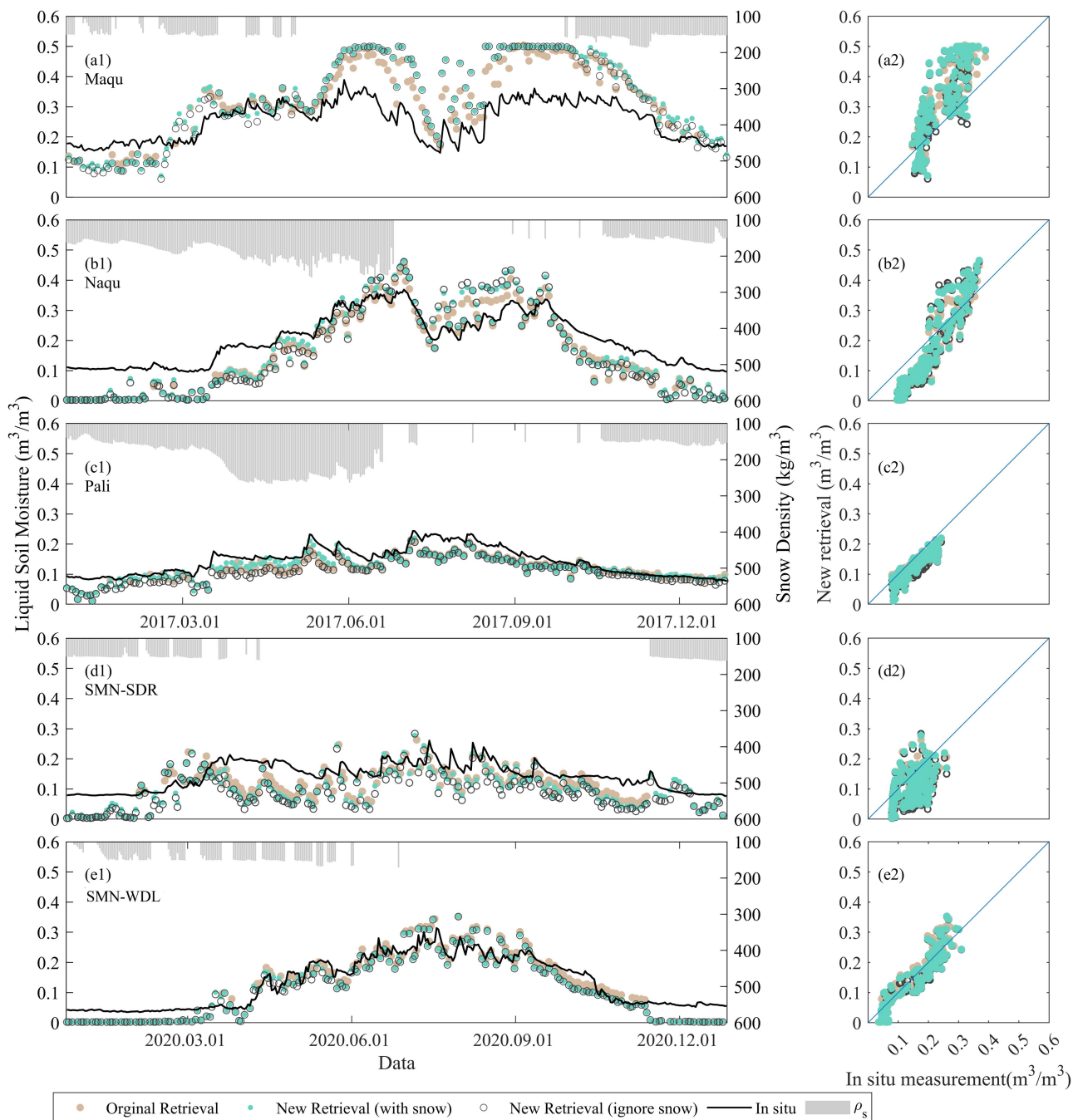


Fig. 5. SM validation with time-series plot and scatter plot for each in-situ network. (a1) Maqu. (b1) Naqu. (c1) Pali. (d1) SMN-SDR. (e1) SMN-WDL. The time series plot contains snow density (kg/m^3) as shown on the right axis (gray bar).

temperature is -0.2°C . SM, which remains stable throughout the year, is largely determined by rainfall, although there are some minor variations.

The SMN-WDL network is located in the western part of the Tibetan Plateau, which has a typical mountain climate. In summer, the area is characterized by high humidity and rainfall, while in winter it is dry and cold [47]. The average annual temperature in the region is -5.1°C . From October, the topsoil begins a regular freeze-thaw cycle, which is completed between December and March. During this freeze-thaw

period, SM decreases steadily and remains at a relatively low level. After April, the soil gradually melted, its liquid water content increased, and the effects of irrigation and rainfall began to show in the changes in the soil's liquid water content.

The SMN-SDR network is located in the agricultural and pastoral mix of Hebei Province and Inner Mongolia [48]. In this region, there are different land types such as grassland, cropland, and bare soil. During winter, there is a decrease in SM at this site, where moisture is consistently low. SM begins to increase

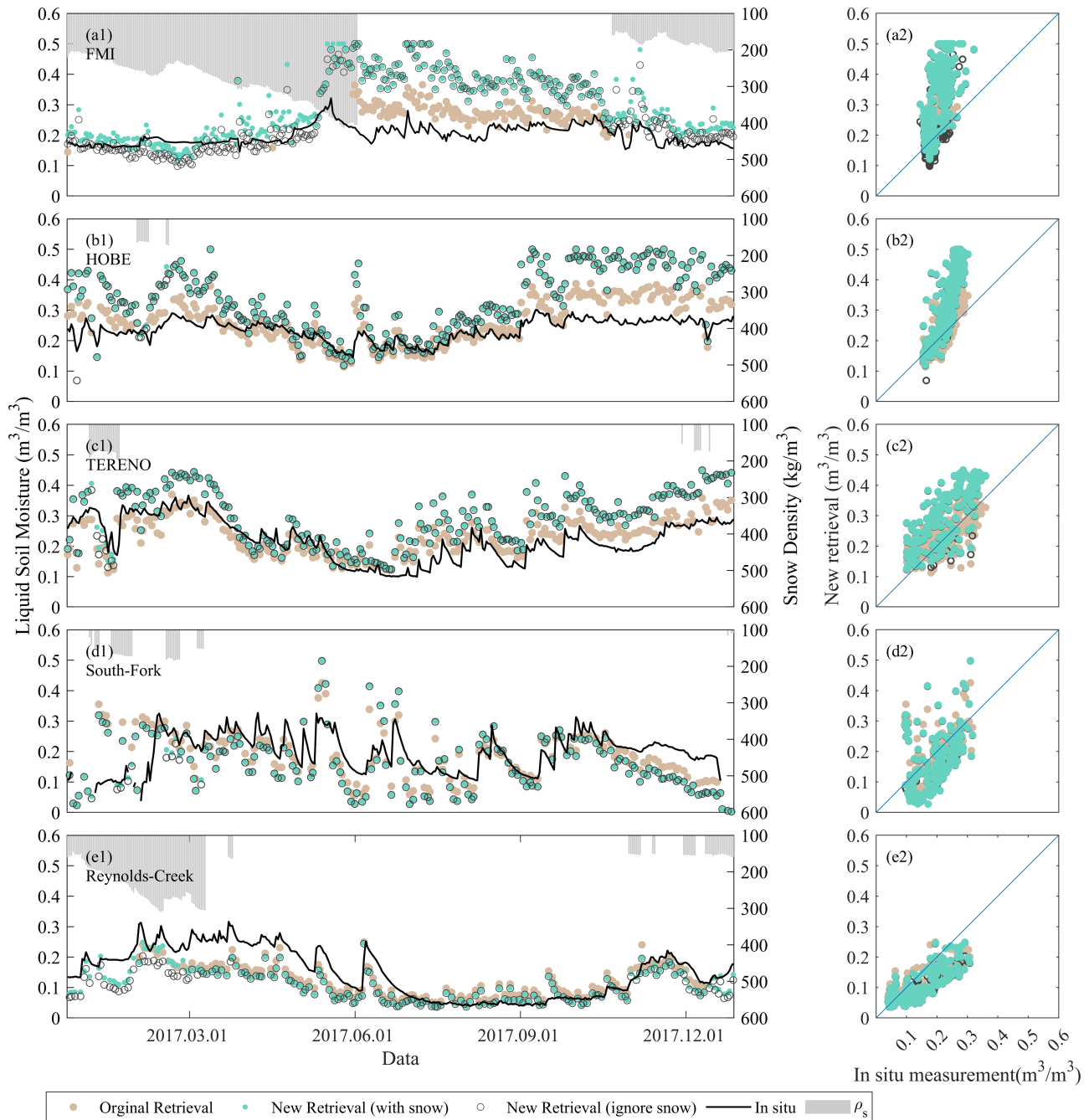


Fig. 6. SM validation with time-series plot and scatter plot for each in-situ network. (a1) FMI. (b1) HOBE. (c1) TERENO. (d1) South-Fork. (e1) Reynolds-Creek. The time series plot contains snow density (kg/m^3) as shown on the right axis (gray bar).

during the transition from winter to spring, and flora expansion is evident during the growing season.

At the FMI site in Finland, which is characterized by a long period of soil freezing [49], SMAP has no SM data during the freezing period. The SMAP product provides approximately 150 days of effective SM data per year. In comparison, our retrieval results yield approximately 350 days per year. Ignoring the effect of snowpack leads to an underestimation of SM.

Despite the correlation of only 0.666 between our retrievals and the in-situ data, the annual variations of SM

were revealed. Even the changes in unfrozen SM during the frost season were effectively captured, showing a high degree of agreement with the in-situ observation. Compared to SMAP and sites, our results from June to October are slightly overestimated.

The estimated SM was compared with in-situ measurements, with an R value of 0.76. The unbiased root mean square error (ubRMSE) was $0.056 \text{ m}^3/\text{m}^3$, and the total bias was $0.011 \text{ m}^3/\text{m}^3$, indicating an underestimation of the SM content. For networks with periods of freezing temperatures, our

TABLE II
STATISTICAL VALIDATION RESULTS AT 17 SOIL MOISTURE NETWORKS

Network	New retrieval					SMAP				
	N	Bias (m ³ /m ³)	RMSE (m ³ /m ³)	ubRMSE (m ³ /m ³)	R	N	Bias (m ³ /m ³)	RMSE (m ³ /m ³)	ubRMSE (m ³ /m ³)	R
Maqu	181	0.076	0.116	0.087	0.838	144	0.092	0.098	0.033	0.857
Naqu	181	-0.036	0.075	0.065	0.948	126	0.011	0.060	0.059	0.916
Pali	181	-0.023	0.030	0.019	0.903	150	-0.015	0.032	0.028	0.910
SMN-SDR	204	-0.044	0.064	0.046	0.582	148	-0.015	0.056	0.054	0.370
SMN-WDL	181	-0.018	0.039	0.034	0.947	106	0.065	0.033	0.056	0.882
FMI	353	0.094	0.127	0.085	0.666	136	0.074	0.067	0.031	0.222
HOBE	268	0.098	0.125	0.078	0.858	256	0.027	0.051	0.043	0.852
Kyeamba	182	0.052	0.103	0.089	0.725	182	0.055	0.084	0.064	0.740
Yanco	182	-0.005	0.058	0.057	0.604	182	0.035	0.062	0.051	0.635
REMEDHUS	180	-0.045	0.059	0.038	0.680	180	-0.019	0.042	0.037	0.691
TERENO	223	0.071	0.093	0.060	0.736	219	0.011	0.050	0.048	0.721
Fort-Cobb	181	-0.038	0.053	0.036	0.871	180	-0.020	0.035	0.029	0.878
Little-Washita	181	-0.019	0.036	0.030	0.876	180	-0.002	0.024	0.024	0.879
South-Fork	177	-0.028	0.084	0.079	0.479	159	-0.007	0.069	0.069	0.483
St.-Josephs	179	0.083	0.118	0.084	0.637	161	0.066	0.080	0.046	0.812
Reynolds-Creek	188	-0.039	0.059	0.044	0.841	157	-0.027	0.052	0.044	0.849
Walnut-Gulch	185	0.003	0.023	0.023	0.791	185	0.032	0.042	0.026	0.787
Overall	200	0.011	0.074	0.056	0.760	167	0.021	0.056	0.044	0.735

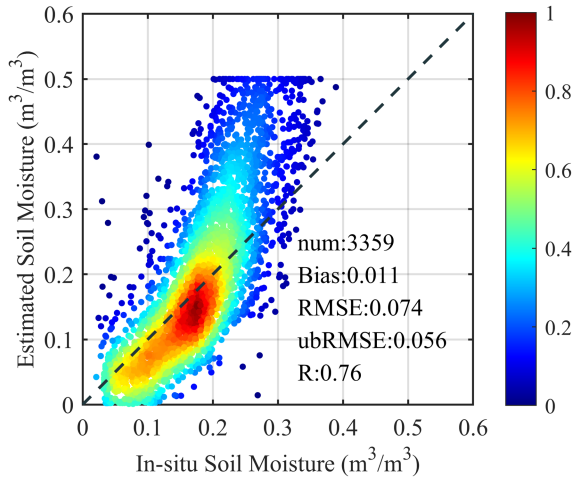


Fig. 7. Joint density scatter plot of measurement SM (x-axis) against retrieval SM (y-axis).

retrievals show a better correlation than SMAP. The variation of SM with seasonal changes is evident from the results.

C. Spatial Distribution of Unfrozen Water Content

Given the verified moderate-to-high accuracy, the global spatial distribution of the annual mean value of unfrozen water content at soil temperatures below 0°C in 2017 was determined (Fig. 8). Also, scatter density plots of temperature and SM were drawn (Fig. 9).

Soil freezing below 0°C has a major effect on the distribution and content of unfrozen liquid water in the soil. This phenomenon is particularly evident in places above 30°N latitude. In these regions, the annual average unfrozen water content remains

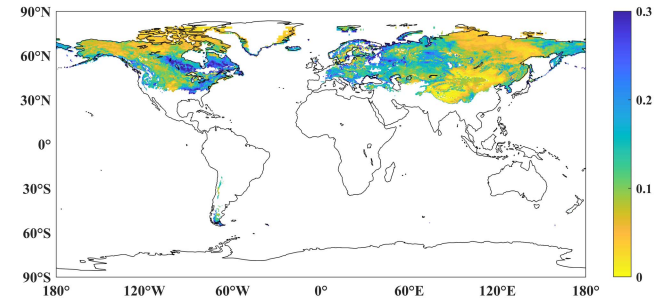


Fig. 8. Spatial distribution of unfrozen water content.

at a relatively low level, with most parts registering less than 0.2 m³/m³.

Fig. 9 provides a better understanding of the correlation between soil unfrozen water content and soil temperature. The freezing process begins when the soil temperature falls below 0°C. As the ambient temperature decreases, the soil undergoes a phenomenon where significant amounts of water freeze, resulting in a reduction in the unfrozen water content. As a result, the remaining unfrozen water reaches a state of equilibrium.

The observed shift is of remarkable magnitude, especially over the temperature range from freezing to -5°C. However, even at very low temperatures, such as -30°C, the soil contains only a minimal amount of unfrozen water.

This study provides a reliable solution for retrieving the unfrozen liquid water. It also serves as a guide for future monitoring of liquid water content in permafrost and seasonal frozen ground regions around the globe.

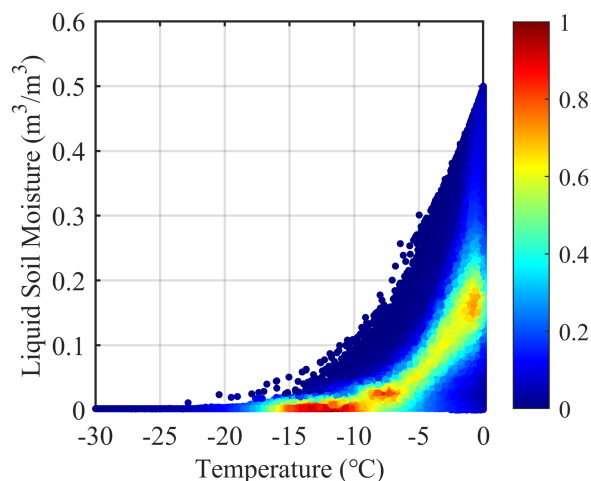


Fig. 9. Joint density scatter plot of soil temperature (x -axis) against liquid SM (y -axis).

D. Discussion

Over the past few decades, the cost and convenience of SM measurement equipment have improved significantly due to the advent of electromagnetic measurement technology and the rapid progress of the semiconductor industry. Significant progress has been made in the measurement of SM.

Existing technologies suitable for frozen soils include time domain reflectometry (TDR) and nuclear magnetic resonance. TDR is used to determine the total dielectric permittivity of the soil. This value is based on the velocity of the transverse electromagnetic wave. It is currently widely used to measure SM content [50]. TDR is one of the most popular techniques used to measure SM content. The dielectric constants of soils with different water contents differ significantly [51]. A number of factors can interfere with the sensor's estimation of the permittivity in frozen ground, including moisture content, ice content, soil structure, and bulk density [52]. In addition, TDR tends to use fixed empirical parameters to convert the measured dielectric permittivity to liquid water content. Due to the difference in molecular structure and state, there is a difference in dielectric constant between free and bound water. It may not account for the difference in dielectric constants between these, or it may ignore the presence of ice in the soil. Therefore, it will theoretically give an equivalent liquid water content instead of the true unfrozen water content, although the difference may not be significant. Strictly speaking, the results of in-situ measurements are not sufficient to validate the retrieval inference of unfrozen water content, which can only be regarded as a point of reference in this article.

In this study, the retrieval of all-season liquid SM revealed that ignoring the effect of snow accumulation leads to an underestimation of liquid SM. This is consistent with the findings of Lemmetyinen et al. [53], who found that ignoring the influence of snow can result in a 35% reduction in the estimations of the local soil dielectric constant, a parameter closely related to SM content. Consequently, an underestimation of the soil dielectric constant will inevitably lead to lower estimates of the liquid

SM. In a previous study, Kumawat et al. [54] addressed the problem of estimating SM of unfrozen soil under snow-covered ground in the United States using the SNODAS snow density dataset. Concurrently, we extended this idea by estimating the liquid SM under both frozen and unfrozen soil globally, using the ERA5 LAND snow density data. Our new validation efforts, using data from FMI sites, showed that snow densities above 200 kg/m^3 can lead to an underestimation of liquid SM by more than 20%. It is important to note that our study did not directly evaluate the accuracy of the snow density data. The direct impact of snow density accuracy on liquid SM retrievals remains unexplored in our research. Therefore, accurate global snow density measurements are crucial for future studies, which should aim to retrieve snow depth, snow density, and liquid SM simultaneously, requiring a satellite mission endowed with both multiangular and multifrequency capabilities.

V. CONCLUSION

Monitoring global shifts in liquid SM beneath both unfrozen and frozen soils can significantly improve the understanding of SM variations in both seasonal frozen ground and permafrost. In this study, we propose an all-season liquid SM retrieval method using SMAP L-band brightness temperature data. This method incorporates the Zhang-Zhao dielectric model, applicable to frozen/thawed soils, into a single-channel SM retrieval algorithm, exploiting the penetration capability of L-band into vegetation and dry snow. Our approach successfully retrieved liquid SM across different seasons on a global scale, highlighting discernible differences in SM patterns between seasonal frozen ground and permafrost. It is also found that the omission of snow cover can lead to an underestimation of liquid water content. Validation results based on in-situ networks around the world confirmed the high accuracy of the method. Despite these achievements, the study was limited to an SCA, and the applicability of the Zhang-Zhao model to other SM retrieval methods needs to be further investigated.

ACKNOWLEDGMENT

The authors would like to thank the NSIDC for providing SMAP TB and SM products.

REFERENCES

- [1] Y.-A. Liou and A. W. England, "A land-surface process/radiobrightness model with coupled heat and moisture transport for freezing soils," *IEEE Trans. Geosci. Remote Sens.*, vol. 36, no. 2, pp. 669–677, Mar. 1998, doi: [10.1109/36.662747](https://doi.org/10.1109/36.662747).
- [2] A. Yang, D. Zheng, J. Wen, X. Lu, Y. Yang, and Q. Fu, "Progress on L-band microwave radiometry observation and soil moisture retrieval over the Tibetan Plateau," *Remote Sens. Technol. Appl.*, vol. 36, no. 5, pp. 983–996, 2021, doi: [10.11873/j.issn.1004-0323.2021.5.0983](https://doi.org/10.11873/j.issn.1004-0323.2021.5.0983).
- [3] D. Zheng et al., "Impacts of Noah model physics on catchment scale runoff simulations," *J. Geophysical Res. Atmos.*, vol. 121, no. 2, pp. 807–832, 2016.
- [4] T. J. Zhao, L. M. Jiang, S. J. Zhao, L. N. Chai, and R. Jin, "A new soil freeze/thaw discriminant algorithm using AMSR-E passive microwave imagery," *Hydrological Processes*, vol. 25, no. 11, pp. 1704–1716, 2011.
- [5] T. J. Zhao et al., "Soil moisture experiment in the Luan River supporting new satellite mission opportunities," *Remote Sens. Environ.*, vol. 240, 2020, Art. no. 111680, doi: [10.1016/j.rse.2020.111680](https://doi.org/10.1016/j.rse.2020.111680).

- [6] E. G. Njoku, T. J. Jackson, V. Lakshmi, T. K. Chan, and S. V. Nghiem, "Soil moisture retrieval from AMSR-E," *IEEE Trans. Geosci. Remote Sens.*, vol. 41, no. 2, pp. 215–229, Feb. 2003.
- [7] T. J. Jackson et al., "Validation of advanced microwave scanning radiometer soil moisture products," *IEEE Trans. Geosci. Remote Sens.*, vol. 48, no. 12, pp. 4256–4272, Dec. 2010.
- [8] J. P. Wigneron et al., "Modelling the passive microwave signature from land surfaces: A review of recent results and application to the L-band SMOS & SMAP soil moisture retrieval algorithms," *Remote Sens. Environ.*, vol. 192, pp. 238–262, 2017.
- [9] Y. H. Kerr, P. Waldteufel, J.-P. Wigneron, J. Martinuzzi, J. Font, and M. Berger, "Soil moisture retrieval from space: The Soil Moisture and Ocean Salinity (SMOS) mission," *IEEE Trans. Geosci. Remote Sens.*, vol. 39, no. 8, pp. 1729–1735, Aug. 2001, doi: [10.1109/36.942551](https://doi.org/10.1109/36.942551).
- [10] Y. Bai et al., "A soil moisture retrieval method for reducing topographic effect: A case study on the Qinghai–Tibetan Plateau with SMOS data," *IEEE J. Sel. Topics Appl. Earth Observ. Remote Sens.*, vol. 16, pp. 4276–4286, Apr. 2023, doi: [10.1109/JSTARS.2023.3264572](https://doi.org/10.1109/JSTARS.2023.3264572).
- [11] D. Entekhabi, T. J. Jackson, E. Njoku, P. O'Neill, and J. Entin, "Soil moisture active/passive (SMAP) mission concept," *Proc. SPIE*, vol. 7085, 2008, Art. no. 70850H.
- [12] Z. Peng et al., "First mapping of polarization-dependent vegetation optical depth and soil moisture from SMAP L-band radiometry," *Remote Sens. Environ.*, vol. 302, 2024, Art. no. 113970, doi: [10.1016/j.rse.2023.113970](https://doi.org/10.1016/j.rse.2023.113970).
- [13] T. J. Zhao, "Recent advances of L-band application in the passive microwave remote sensing of soil moisture and its prospects," *Prog. Geography*, vol. 37, no. 2, pp. 198–213, 2018, doi: [10.18306/dlkxjz.2018.02.003](https://doi.org/10.18306/dlkxjz.2018.02.003).
- [14] M. C. Dobson, F. T. Ulaby, M. T. Hallikainen, and M. A. El-rayes, "Microwave dielectric behavior of wet soil-part II: Dielectric mixing models," *IEEE Trans. Geosci. Remote Sens.*, vol. GE-23, no. 1, pp. 35–46, Jan. 1985.
- [15] V. Mironov, Y. Kerr, J.-P. Wigneron, L. Kosolapova, and F. Demontoux, "Temperature- and texture-dependent dielectric model for moist soils at 1.4 GHz," *IEEE Geosci. Remote Sens. Lett.*, vol. 10, no. 3, pp. 419–423, May 2013.
- [16] M. Schwank, M. Stahli, H. Wydler, J. Leuenberger, and H. Fluhler, "Microwave L-band emission of freezing soil," *IEEE Trans. Geosci. Remote Sens.*, vol. 42, no. 6, pp. 1252–1261, Jun. 2004.
- [17] J. R. Birchak, C. G. Gardner, J. E. Hipp, and J. M. Victor, "High dielectric constant microwave probes for sensing soil moisture," *Proc. IEEE*, vol. 62, no. 1, pp. 93–98, Jan. 1974.
- [18] V. L. Mironov, R. D. De Roo, and I. V. Savin, "The process of unfrozen water freezing with decreasing temperature studied by dielectric measurement in the case of an Arctic soil," in *Proc. IEEE Int. Geosci. Remote Sens. Symp.*, 2010, pp. 4423–4425, doi: [10.1109/IGARSS.2010.5652122](https://doi.org/10.1109/IGARSS.2010.5652122).
- [19] V. L. Mironov and Y. I. Lukin, "A physical model of dielectric spectra of thawed and frozen bentonitic clay within the frequency range from 1 to 15 GHz," *Russian Phys. J.*, vol. 53, no. 9, pp. 956–963, 2011.
- [20] V. L. Mironov, R. D. De Roo, and I. V. Savin, "Temperature-dependable microwave dielectric model for an arctic soil," *IEEE Trans. Geosci. Remote Sens.*, vol. 48, no. 6, pp. 2544–2556, Jun. 2010.
- [21] V. Mironov and I. Savin, "A temperature-dependent multi-relaxation spectroscopic dielectric model for thawed and frozen organic soil at 0.05–15 GHz," *Phys. Chem. Earth, Parts A/B/C*, vol. 83–84, pp. 57–64, 2015.
- [22] V. L. Mironov, L. G. Kosolapova, Y. I. Lukin, A. Y. Karavayev, and I. P. Molostov, "Temperature- and texture-dependent dielectric model for frozen and thawed mineral soils at a frequency of 1.4GHz," *Remote Sens. Environ.*, vol. 200, pp. 240–249, 2017, doi: [10.1016/j.rse.2017.08.007](https://doi.org/10.1016/j.rse.2017.08.007).
- [23] V. L. Mironov, A. Y. Karavayev, Y. I. Lukin, and I. P. Molostov, "A dielectric model of thawed and frozen Arctic soils considering frequency, temperature, texture and dry density," *Int. J. Remote Sens.*, vol. 41, no. 10, pp. 3845–3865, 2020.
- [24] A. Mavrovic, R. P. Lara, A. Berg, and A. Roy, "Soil dielectric characterization during freeze–thaw transitions using L-band coaxial and soil moisture probes," *Hydrol. Earth Syst. Sci.*, vol. 25, pp. 1117–1131, 2021.
- [25] L. Zhang, T. Zhao, L. Jiang, and S. Zhao, "Estimate of phase transition water content in freeze–thaw process using microwave radiometer," *IEEE Trans. Geosci. Remote Sens.*, vol. 48, no. 12, pp. 4248–4255, Dec. 2010.
- [26] T. J. Zhao et al., "Measurement and modeling of multi-frequency microwave emission of soil freezing and thawing processes," in *Proc. Prog. Electromagn. Res. Symp.*, 2018, pp. 31–36, doi: [10.23919/PIERS.2018.8597699](https://doi.org/10.23919/PIERS.2018.8597699).
- [27] S. Wu, T. Zhao, J. Pan, H. Xue, L. Zhao, and J. Shi, "Improvement in modeling soil dielectric properties during freeze-thaw transitions," *IEEE Geosci. Remote Sens. Lett.*, vol. 19, Feb. 2022, Art. no. 2001005, doi: [10.1109/LGRS.2022.3154291](https://doi.org/10.1109/LGRS.2022.3154291).
- [28] T. Mo, B. J. Choudhury, T. J. Schmugge, J. R. Wang, and T. J. Jackson, "A model for microwave emission from vegetation-covered fields," *J. Geophysical Res.: Oceans*, vol. 87, no. C13, pp. 11229–11237, 1982, doi: [10.1029/JC087iC13p11229](https://doi.org/10.1029/JC087iC13p11229).
- [29] W. A. Dorigo et al., "The International Soil Moisture Network: A data hosting facility for global in situ soil moisture measurements," *Hydrol. Earth Syst. Sci.*, vol. 15, no. 5, pp. 1675–1698, 2011, doi: [10.5194/hess-15-1675-2011](https://doi.org/10.5194/hess-15-1675-2011).
- [30] K. Yang et al., "A multiscale soil moisture and freeze-thaw monitoring network on the third pole," *Bull. Amer. Meteorological Soc.*, vol. 94, no. 12, pp. 1907–1916, 2013.
- [31] A. Colliander et al., "Validation of SMAP surface soil moisture products with core validation sites," *Remote Sens. Environ.*, vol. 191, pp. 215–231, 2017, doi: [10.1016/j.rse.2017.01.021](https://doi.org/10.1016/j.rse.2017.01.021).
- [32] J. Zheng et al., "Assessment of 24 soil moisture datasets using a new in situ network in the Shandian River Basin of China," *Remote Sens. Environ.*, vol. 271, 2022, Art. no. 112891, doi: [10.1016/j.rse.2022.112891](https://doi.org/10.1016/j.rse.2022.112891).
- [33] T. Hengl et al., "SoilGrids250m: Global gridded soil information based on machine learning," *PLoS One*, vol. 12, no. 2, 2017, Art. no. e0169748, doi: [10.1371/journal.pone.0169748](https://doi.org/10.1371/journal.pone.0169748).
- [34] T. R. Loveland et al., "Development of a global land cover characteristics database and IGBP DISCover from 1 km AVHRR data," *Int. J. Remote Sens.*, vol. 21, no. 6–7, pp. 1303–1330, 2000.
- [35] J. M. Sabater, "ERA5-Land hourly data from 1981 to present. Copernicus climate change service (C3S) climate data store (CDS)," Tech. Rep., Eur. Centre Medium-Range Weather Forecasts, Eur. Union, 2019.
- [36] T. J. Jackson, "III. Measuring surface soil moisture using passive microwave remote sensing," *Hydrological Processes*, vol. 7, pp. 139–152, 1993.
- [37] J. R. Wang and B. J. Choudhury, "Remote sensing of soil moisture content, over bare field at 1.4 GHz frequency," *J. Geophysical Res. Oceans*, vol. 86, no. C6, pp. 5277–5282, 1981.
- [38] T. Mo and T. J. Schmugge, "A parameterization of the effect of surface roughness on microwave emission," *IEEE Trans. Geosci. Remote Sens.*, vol. GE-25, no. 4, pp. 481–486, Jul. 1987, doi: [10.1109/tgrs.1987.289860](https://doi.org/10.1109/tgrs.1987.289860).
- [39] J. R. Wang, P. E. Neill, T. J. Jackson, and E. T. Engman, "Multifrequency measurements of the effects of soil moisture, soil texture, and surface roughness," *IEEE Trans. Geosci. Remote Sens.*, vol. 21, no. 1, pp. 44–51, Jan. 1983, doi: [10.1109/tgrs.1983.350529](https://doi.org/10.1109/tgrs.1983.350529).
- [40] M. Schwank et al., "Snow density and ground permittivity retrieved from L-band radiometry: A synthetic analysis," *IEEE J. Sel. Topics Appl. Earth Observ. Remote Sens.*, vol. 8, no. 8, pp. 3833–3845, Aug. 2015, doi: [10.1109/JSTARS.2015.2422998](https://doi.org/10.1109/JSTARS.2015.2422998).
- [41] T. J. Zhao et al., "Parametric exponentially correlated surface emission model for L-band passive microwave soil moisture retrieval," *Phys. Chem. Earth, Parts A/B/C*, vol. 83–84, pp. 65–74, 2015, doi: [10.1016/j.pce.2015.04.001](https://doi.org/10.1016/j.pce.2015.04.001).
- [42] S. Ersahin, H. Gunal, T. Kutlu, B. Yetgin, and S. Coban, "Estimating specific surface area and cation exchange capacity in soils using fractal dimension of particle-size distribution," *Geoderma*, vol. 136, no. 3, pp. 588–597, 2006, doi: [10.1016/j.geoderma.2006.04.014](https://doi.org/10.1016/j.geoderma.2006.04.014).
- [43] P. O'Neill, R. Bindlish, S. Chan, E. Njoku, and T. Jackson, "Algorithm theoretical basis document level 2 & 3 soil moisture (passive) data products," Rev. C. In: SMAP Project. Jet Propulsion Laboratory, Pasadena, CA, USA, 2018.
- [44] T. J. Jackson and T. J. Schmugge, "Vegetation effects on the microwave emission of soils," *Remote Sens. Environ.*, vol. 36, no. 3, pp. 203–212, Jun. 1991.
- [45] Z. Su et al., "The Tibetan Plateau observatory of plateau scale soil moisture and soil temperature (Tibet-Obs) for quantifying uncertainties in coarse resolution satellite and model products," *Hydrol. Earth Syst. Sci.*, vol. 15, no. 7, 2017, Art. no. 2303.
- [46] Y. Chen et al., "Evaluation of SMAP, SMOS, and AMSR2 soil moisture retrievals against observations from two networks on the Tibetan Plateau," *J. Geophysical Res.: Atmos.*, vol. 122, pp. 5780–5792, 2017.
- [47] J. Zheng et al., "Use of a new Tibetan Plateau network for permafrost to characterize satellite-based products errors: An application to soil moisture and freeze/thaw," *Remote Sens. Environ.*, vol. 300, 2024, Art. no. 113899, doi: [10.1016/j.rse.2023.113899](https://doi.org/10.1016/j.rse.2023.113899).
- [48] T. Zhao et al., "Comprehensive remote sensing experiment of water cycle and energy balance in the Shandian river basin," *J. Remote Sens.*, vol. 25, no. 2, pp. 871–887, 2020, doi: [10.11834/jrs.20219401](https://doi.org/10.11834/jrs.20219401).
- [49] S. Bircher, M. Andreasen, J. Vuollet, J. Vehviläinen, and Y. H. Kerr, "Soil moisture sensor calibration for organic soil surface layers," *Geoscientific Instrum. Methods Data Syst. Discuss.*, vol. 5, no. 2, pp. 447–493, 2015.

- [50] H. Fellner-Feldegg, "Measurement of dielectrics in the time domain," *J. Phys. Chem.*, vol. 73, no. 3, pp. 616–623, 1969.
- [51] G. C. Topp, J. L. Davis, and A. P. Annan, "Electromagnetic determination of soil water content: Measurements in coaxial transmission lines," *Water Resour. Res.*, vol. 16, no. 3, pp. 574–582, 1980.
- [52] K. Watanabe and M. Mizoguchi, "Amount of unfrozen water in frozen porous media saturated with solution," *Cold Regions Sci. Technol.*, vol. 34, no. 2, pp. 103–110, 2002.
- [53] J. Lemmetyinen et al., "Snow density and ground permittivity retrieved from L-band radiometry: Application to experimental data," *Remote Sens. Environ.*, vol. 180, pp. 377–391, 2016, doi: [10.1016/j.rse.2016.02.002](https://doi.org/10.1016/j.rse.2016.02.002).
- [54] D. Kumawat, M. Olyaei, L. Gao, and A. Ebtehaj, "Passive microwave retrieval of soil moisture below snowpack at L-band using SMAP observations," *IEEE Trans. Geosci. Remote Sens.*, vol. 60, Oct. 2022, Art. no. 4415216, doi: [10.1109/TGRS.2022.3216324](https://doi.org/10.1109/TGRS.2022.3216324).



Chi Wang received the B.S. degree in surveying and mapping engineering from Nanjing Forestry University, Nanjing, China, in 2019. He is currently working toward the M.S. degree in resources and environmental engineering with Henan Polytechnic University, Jiaozuo, China.

His research interests include microwave remote sensing of all-season liquid soil moisture retrieval.



Na Yang received the B.S. degree in photogrammetry and remote sensing from Wuhan University, Wuhan, China, in 2003, M.S. degree in cartography and geographic information systems from Ocean University of China, Qingdao, China, in 2006, and the Ph.D. degree in photogrammetry and remote sensing from Wuhan University, Wuhan, China, in 2010.

In 2015, she was a Visiting Scientist with the School of Archaeology, Geography and Environmental Science, University of Reading, Reading, U.K. She is currently an Associate Professor with Henan Poly-

technic University, Jiaozuo, China. Her research interests include microwave remote sensing of soil moisture and data assimilation.



Tianjie Zhao (Senior Member, IEEE) received the B.S. and Ph.D. degrees in cartography and geographic information systems from Beijing Normal University, Beijing, China, in 2007 and 2012, respectively.

From 2010 to 2012, he was a Visiting Scientist with the Hydrology and Remote Sensing Laboratory, Agricultural Research Service U.S. Department of Agriculture, Beltsville, MD, USA. He is currently a Research Professor with the State Key Laboratory of Remote Sensing Science, Aerospace Information Research Institute, Chinese Academy of Sciences,

Beijing, China. His research interests include microwave remote sensing of soil moisture and its freeze-thaw process.

Dr. Zhao was the recipient of the scholarship award for excellent doctoral student granted by the Ministry of Education of China in 2011, the Young Scientist Award from the International Union of Radio Science (URSI) in 2014, the Young Scientist Award from Progress in Electromagnetics Research Symposium (PIERS) in 2018, and the Li Xiaowen Youth Award in Remote Sensing Science in 2023.



Huazhu Xue received the Ph.D. degree in cartography and geographic information systems in the area of quantitative remote sensing from the School of Geography, Beijing Normal University, Beijing, China, in 2012.

Since 2012, he has been an Associate Professor with the School of Surveying and Land Information Engineering, Henan Polytechnic University, Jiaozuo, China. His research interests include vegetation parameters inversion, satellite image processing, and GIS applications.



Zhiqing Peng is currently working toward the Ph.D. degree in cartography and geographic information Systems at the Aerospace Information Research Institute, Chinese Academy of Sciences (CAS), Beijing, China.

His research interests include microwave remote sensing of soil moisture retrieval and data fusion at L-band.



Jingyao Zheng is currently working toward the Ph.D. degree with the College of Hydrology and Water Resources, Hohai University, Nanjing, China.

His research interests include the spatial downscaling of satellite-based soil moisture for hydrological applications.



Jinmei Pan received the B.S. and M.S. degrees in cartography and geographic information system from Beijing Normal University, Beijing, China, in 2009 and 2012, respectively, and the Ph.D. degree in geodetic science from The Ohio State University, Columbus, OH, USA, in 2017.

Since graduation, she joined the State Key Laboratory of Remote Sensing Science, Beijing, China, working as an Assistant Researcher from 2017 to 2023. Before 2020, he was with the Institute of Remote Sensing and Digital Earth, Chinese Academy of

Sciences (CAS), Beijing, China. She is currently with the Aerospace Information Research Institute, CAS. She is currently situated with the National Space Science Center, CAS. Her research interests at the current stage are snow depth, snow water equivalent and snowmelt estimation supported by passive microwave remote sensing and snow process model.



Panpan Yao received the B.E. and M.E. degrees in cartography and geographic information engineering from China University of Petroleum (East China), Qingdao, China, in 2011 and 2014, respectively, and the Ph.D. degree in cartography and geography information system from the Institute of Remote Sensing and Digital Earth, Chinese Academy of Sciences (CAS), Beijing, China, in 2018.

From 2018 to 2020, she was a Postdoctor with the Department of Earth System Science, Tsinghua University. She is currently an Assistant Researcher with the State Key Laboratory of Remote Sensing Science, Aerospace Information Research Institute, CAS. Her research interests include microwave remote sensing of soil moisture and application in hydrology.



Xiaowen Gao received the B.S. degree in resources and environmental engineering from Wuhan University of Technology, Wuhan, China, in 2018. She is currently working toward the M.S. degree in resources and environmental engineering with the University of Chinese Academy of Sciences, Beijing, China, and also with the State Key Laboratory of Remote Sensing Science, Aerospace Information Research Institute, Chinese Academy of Sciences, Beijing, China.

Her research interests include snow microwave remote sensing and snow density estimation.



Hongbo Yan received the Ph.D. degree in geological resources and geological engineering from Guilin University of Technology, Guilin, China, in 2020.

She is currently an Associate Professor with the College of Geomatics and Geoinformatics, Guilin University of Technology. She has authored or coauthored more than 20 peer-reviewed publications. Her research interests are in integrating optical remote sensing and microwave remote sensing with modeling and algorithm development for retrievals of land surface parameters.



Peilin Song was born in Henan, China. He received the B.S. degree in geography information system from Northwest Agriculture and Forest University, Yangling, China, in 2014, and the Ph.D. degree in applied remote sensing from Zhejiang University, Hangzhou, China, in 2019.

From 2019 to 2022, he was a Postdoctoral Researcher with the Institute of Geographic Sciences and Natural Resources Research, Chinese Academy of Sciences, Beijing, China. Since 2022, he has been an Assistant Professor with Xi'an Jiaotong University, Xi'an, China.

His research interests include microwave remote sensing, soil moisture retrieval and downscaling algorithms, land surface temperature downscaling, and multisource data fusion techniques.



Yuei-An Liou (Senior Member, IEEE) received the B.S. degree in electrical engineering (EE) from National Sun Yat-sen University, Kaohsiung, Taiwan, in 1987, and the M.S.E. degree in EE, the M.S. degree in atmospheric and space sciences, and the double Ph.D. degrees in EE and atmospheric, oceanic, and space sciences from the University of Michigan, Ann Arbor, MI, USA, in 1992, 1994, and 1996, respectively.

He is currently a Distinguished Professor with the Center for Space and Remote Sensing Research, National Central University, Taoyuan, Taiwan. He has authored more than 150 research articles. His journal papers' H-index is 44 (Google Scholar) with more than 6400 citations (including self-citations). His research interests include GPS meteorology and ionosphere, remote sensing of the atmosphere, land surface, and polar ice, and land surface processes modeling.

Dr. Liou is a Foreign Member of the Russian Academy of Engineering Sciences and a member of the International Academy of Astronautics. He has actively contributed to the scientific community and many journals as an editor, an editorial advisory board member, a guest editor, and a reviewer.



Jiancheng Shi (Fellow, IEEE) received the B.A. degree in geology and geological engineering from the University of Lanzhou, Lanzhou, China, in 1982, and the M.A. and Ph.D. degrees in geography from the University of California, Santa Barbara (UCSB), Santa Barbara, CA, USA, in 1987 and 1991, respectively.

He was a Research Professor with the Institute for Computational Earth System Sciences, UCSB. In 2010, he became the Director and Senior Research Scientist with the State Key Laboratory of Remote Sensing Science, sponsored by the Aerospace Information Research Institute, Chinese Academy of Sciences and Beijing Normal University, Beijing, China. He was the PI of the Water Cycle Observation Mission (WCOM). He is currently a Senior Research Scientist with the National Space Science Center, Chinese Academy of Sciences, Beijing, China. His research interests include microwave remote sensing and global water cycle studies.

He has published more than 500 papers cited nearly 14 000 times. He has made significant contributions to both active and passive microwave remote sensing.